Synchronization and attractors in a model simulating social jetlag

Flávia M. Ruziska*, Iberê L. Caldas

Instituto de Física, Universidade de São Paulo, Rua do Matão, 1371, São Paulo 05508-090, SP, Brazil

A R T I C L E   I N F O

A B S T R A C T

Much work has been done to investigate social jetlag, a misalignment between the biological clock and the social agenda, related to exposition to dirent light inputs, that causes several health issues. To investigate synchronization and attractors due to a sequence of light inputs, we introduce an extension of a model, previously used to describe jetlag caused by a single change in the light input. The synchronization to the light input is sensitive to the control parameters of the system and to the light input periods. Depending on the parameter set, the observed synchronization is with one or another successive light input. Most of the solutions have the period of the light input. However, for some parameters, we also observe higher period, chaotic solutions, and bistability.

© 2021 Elsevier Ltd. All rights reserved.

1. Introduction

The circadian rhythms are 24-hour cycles produced by internal processes and entrained by external stimulus. The master clock of these cycles in mammals is the suprachiasmatic nucleus (SCN). A pathway from the retina to the suprachiasmatic nucleus (SCN) allows the synchronization of circadian rhythms to the solar days [1,2].

Disruptions in the circadian rhythms can implicate several health issues on the short and on the long term. The disruption in the circadian rhythms which most people know is the jetlag. Jetlag occurs when someone travels through time zones, since different time zones have different light-dark cycles [3,4]). Jetlag causes effects like impaired daytime function, general malaise and gastrointestinal disruption in the days immediately following travel [5]. Although these effects are unpleasant and harmful for some groups, there are also other circadian rhythms disruptions that affect many people generating health issues on the long term. For instance, shift-workers (e.g. firemen, doctors on night shifts) usually suffer from disruptions in the circadian rhythms. Empirical evidences indicate the association between these disruptions and negative outcomes related to heart health, metabolic and gastrointestinal health, mental health, and cancer [6–9]. However, not only the shift-workers suffer from disruptions in the circadian rhythms. For example, as Smarr and Schirmer point out in [10], most students experience social jetlag correlated to decreased performance.

Social jetlag is a misalignment between the social dynamic and the endogenous circadian rhythms of one individual. Several studies have been made in order to show the relation between social jetlag and other disorders. For instance, there are relations between social jetlag and depression [11]; also, social jetlag is a risk factor for obesity and related diseases [12]. For these reasons it is important to study models that consider systematic disruptions in the circadian rhythms, and researchers are currently doing works in this area [13]. In this context, in this article we consider that the circadian rhythms are produced by endogenous oscillators that synchronize with the light input cycle.

From the dynamical system point of view, it is interesting to find a simple model that captures the main characteristics of a system. For that reason, here we adopt as base the model introduced in [3], defined by four ODEs and yet able to reproduce the reported experimental data. In [3] it was experimentally shown that mice without arginine vasopressins (AVP) receptors, or mice in which the arginine vasopressins (AVP) was pharmacology blocked, recovered faster from jetlag than regular mice. It is worth mentioning that the substance Arginine-vasopressin (AVP) is synthesized and released from nerve terminals in the central nervous system in the brain. This substance modulates several neuronal functions, for instance, arginine-vasopressin (AVP) is involved in the control of stress, cognitive behaviors and circadian rhythms [14].

In reference [3] the authors studied a scenario similar to a jetlag, with only one shift in the light input. We, on the other hand, are interested in systematic shifts, that emulate the artificial light input of a shift-worker or of a person who suffers from social jetlag. Thus, we extend the model used in [3] for mice jetlag to investigate social jetlag. In fact, similarities between suprachiasmatic

* Corresponding author.
    E-mail addresses: flavia@if.usp.br (F.M. Ruziska), ibere@if.usp.br (I.L. Caldas).

nucleus (SCN) of mamals have been discussed in the literature [15]. We are assuming that changes on the artificial light input represent changes on the routine because nowadays people can control their artificial light input through electrical light. We are interested in understanding how the model solutions (attractors) change when this new type of light input is inserted. We also aim to understand the effect of the variation of the coupling parameter, which accordingly to [3] is related to arginine-vasopressin (AVP).

Exploring the model in a large set of parameters and using techniques that allow us to measure numerically if a time-series is better synchronized with one stimulus or another, we find different scenarios of synchronization depending on the parameter. For most parameters the solutions are period 1 (considering a Poincaré section in which we take one value per week). However, for some parameters, there are solutions of higher periods or chaotic, or even bistable solutions.

In Section 2 we define the model; in Section 3 we present the results first treating one specific light input sequence; in Section 4 we generalize our analyzes, we present the results for a set of light inputs sequences and a range of the coupling parameter; finally in Section 5 we discuss the main results and highlight our conclusions.

2. Model

To describe the suprachiasmatic nucleus (SCN) behavior, that allows the synchronization of circadian rhythms to the solar days [1,2], we use a phase oscillator model introduced in [3]. In this model ϕ_0 is the phase of the oscillator 0, that receives the light input $L(t)$. The oscillator 0 represents the neurons in the suprachiasmatic nucleus (SCN) receiving directly the light. These neurons are called retinorecipent cells, and they are located exclusively in the core of the suprachiasmatic nucleus (SCN). One example of them are the VIP cells or VIP neurons. ϕ_1 and ϕ_2 are the phases of oscillators 1 and 2 which do not receive light directly. However, oscillators 1 and 2 are coupled between themselves and with oscillator 0. The oscillators 1 and 2 represent the cells whose coupling between themselves is incresead by the substance arginine-vasopressin (AVP); due to this reason these cells also are called AVP cells. However, the arginine-vasopresin is not the only substance involved in the coupling, there are others such as the substante GABA. Therefore, we represent the oscillators 1 and 2 coupling by the paramenter K_{couple} that has one component K_{AVP}, associated to argine vasopressin AVP, and other K_c associated to other substances. This model assumes that the output of the suprachiasmatic nucleus is the function $G(\phi_1, \phi_2)$ that is a composition of the phases ϕ_1 and ϕ_2. Finally this total output of the SCN is transmitted to a peripheral oscillator 3, whose phase is named ϕ_3. The output of this peripheral oscillator is given by the function $g_3(\phi_3)$. We focused our analysis on the oscillator 3 because it is the one that receives the total output of the suprachiasmatic nucleus (SCN). For more details of the biological interpretation of the terms see supplementary material of [3]. The model equations are:

$$\frac{d}{dt}\phi_0 = \omega_0 + K_a Z(\phi_0, \varphi_a) L(t) \tag{1}$$

$$\frac{d}{dt}\phi_1 = \omega_1 + K_b Z(\phi_1, \varphi_b) h(\phi_0 + 0.05) + K_{couple} Z(\phi_1, 0) h(\phi_2 + \alpha), \tag{2}$$

$$\frac{d}{dt}\phi_2 = \omega_2 + K_b Z(\phi_2, \varphi_b) h(\phi_0 + 0.05) + (K_{couple}) Z(\phi_2, \alpha) h(\phi_1), \tag{3}$$

$$\frac{d}{dt}\phi_3 = \omega_3 + K_d Z(\phi_3, \varphi_d) G(\phi_1, \phi_2), \tag{4}$$

where,

$$Z(\phi_l, \varphi_l) = -\sin[2\pi(\phi_l + \varphi_l)] \tag{5}$$

$$h = \sin(\pi\phi/\theta), \quad 0 \leq \mod(\phi, 1) \leq \theta; \quad 0 \quad \text{otherwise.} \tag{6}$$

$$G(\phi_1, \phi_2) = \left(\frac{2 + \sin(2\pi\phi_1) + \sin(2\pi\phi_2)}{4} \right) \tag{7}$$

$$g_3 = \sin(2\pi\phi_3) \tag{8}$$

$$\varphi_a = 0.1, \varphi_b = 0.4, \varphi_d = -0.08, \alpha = 0.35, \theta = 0.1 \tag{9}$$

$$K_{couple} = K_{AVP} + K_c \tag{10}$$

$$K_a = 8.0, K_b = 2.7, K_c = 0.6, K_d = 0.5. \tag{11}$$

$$K_{AVP} = 0.7 \text{ represent regular mice} \tag{12}$$

$$K_{AVP} = 0 \text{ represent modified mice without receptors of AVP} \tag{13}$$

In [3] the authors showed that this model reproduces pretty well the experimental data they analyzed. Experimentally, the authors find out that if there are no receptors of arginine-vasopressin (AVP), or when this substance is blocked, the mice recover faster from the jetlag. In the model, the parameter representing this substance is K_{avp}, and the authors verified that if the system is submitted to a light input shift (travel through timezone), it reaches the new equilibrium faster when K_{AVP} (and consequently K_{couple}) is lower. It is worth remembering that in the model adopted $K_{couple} = K_{AVP} + K_c$ represents the coupling between the neurons, the boundaries of the interval in which we vary K_{couple} are the extreme cases studied in [3].

In our work, instead of considering a light input with only one shift to emulate a jetlag scenario as in the original model, we consider periodic shifts in the light input, to emulate a scenario in which there is an abrupt change in the light input weekly. The idea is that this kind of light input is able to represent a sketch from the artificial light input which a shift-worker is used to, or, more generally, of a person who suffers from social jetlag is used to.

We divide the week in two parts: in the first part, the individuals receive the light input A; and in the second part they receive the light input B. Light inputs A and B are both regular, 12 h of light followed by 12 h of dark. However B has a delay of 8 h in relation to A, in other words, B could be associated to a timezone 8 h behind a timezone associated to light input A. The individual spends l days under light input B; and $(7 - l)$ days under light input A. We name the light input through all the week light input $AB(l)$. In Fig. 1 we show a scheme of the light input for the specific case $l = 2.5$.

First we apply the model for a specific value of $l = 2.5$. Next we consider solutions for l in the whole interval $[0,7]$ and parameter K_{couple} in the interval $[0.6, 1.3]$.

3. Results for light input with a shift in weekends

In this subsection we analyze the specific case light input $AB(l = 2.5)$. We could also call this a week-weekend light input, since during the week the light input is equal to light input A and during the weekend it is equal to light input B.

In Fig. 2 we show the function $g_3(\phi_3)$ for three different light inputs (A, B, $AB(l = 2.5)$). This function is defined as
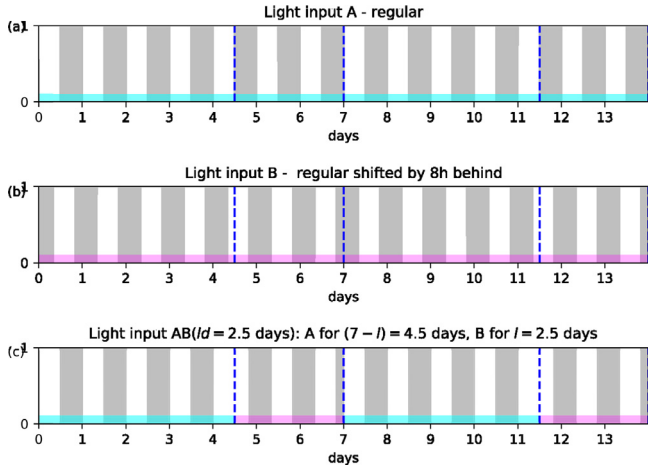
Fig. 1. (a) Light input *A* - regular light input, 12 h of light (−12 to 0) followed by 12 h of dark (0 to 12). (b) Light input *B* 12 h of light (−4 to 8) followed by 12 h of dark (8 to −4), in other words, light input *A* with a delay of 8 h (c) Light input *AB*(*l* = 2.5), light input *A* for 4.5 days followed by light input *B* for 2.5 days.

$g_3(\phi_3) = \sin(2\pi\phi_3)$ where ϕ_3 is the phase of the oscillator 3 of the model, which represents the peripheral oscillator that receives the signal of the SCN.

Analyzing Fig. 2 we notice that as K_{couple} increases the curve for $AB(l = 2.5)$ gets similar to the curve for light input *B*; when $K_{couple} = 1.3$ they almost coincide.

The signal is better synchronized with the light input *B* (weekend) than *A* (week) for $K_{couple} = 1.3$. Since the model is highly non-linear such result can be produced.

Aiming to evaluate numerically how the phase ϕ_3 changes according to different light inputs we introduce the distribution *z* defined as

$$z(\phi_3, \phi_3') = e^{i[2\pi(\phi_3 - \phi_3')]} \tag{14}$$

Table 1
Numerical comparison of $\phi_{3AB(l=2.5)}$ to ϕ_{3A} and ϕ_{3B}.

$R(\phi_{3AB}, \phi_3')$	$\theta(\phi_3, \phi_3')$	ϕ_3'	K_{couple}
0.954	−0.642π	ϕ_{3A}	1.3
0,998	0.024π	ϕ_{3B}	1.3
0.925	−0.292π	ϕ_{3A}	0.6
0.920	0.373π	ϕ_{3B}	0.6

The modulus of the first moment of $z(\phi_3, \phi_3')$ is given by

$$R(\phi_3, \phi_3') = \frac{1}{N}\left|\sum_{i=1}^{N} z_i\right|, \tag{15}$$

which can be understood as a measurement of how much the two phases are synchronized; *N* is the number of points used to evaluate the average. Finally, the mean angle θ of the first moment given by

$$\theta = Arg\left(\frac{1}{N}\sum_{i=1}^{N} z_i\right), \tag{16}$$

and it estimates the mean lag between ϕ_3 and ϕ_3'.

To simplify the notation we call phase ϕ_3 generated by light inputs A, B and AB(l) as ϕ_{3A}, ϕ_{3B} and ϕ_{3AB}, respectively.

In the Table 1 we present the values for *R* and θ fixing ϕ_3 as $\phi_{3AB(l=2.5)}$, considering ϕ_3' as ϕ_{3A} or ϕ_{3B} and the extreme values of K_{couple} 0.6 and 1.3.

These results confirm numerically that, when $K_{couple} = 1.3$, $\phi_{3AB(l=2.5)}$ generated by the light input $AB(l = 2.5)$ is better synchronized with ϕ_{3B} generated by light input *B* than with ϕ_{3A} generated by light input *A*. For $K_{couple} = 0.6$ the differences are substantially smaller.

One important question is if the results which we find for *l* = 2.5 are an exception or if they are common in the parameter
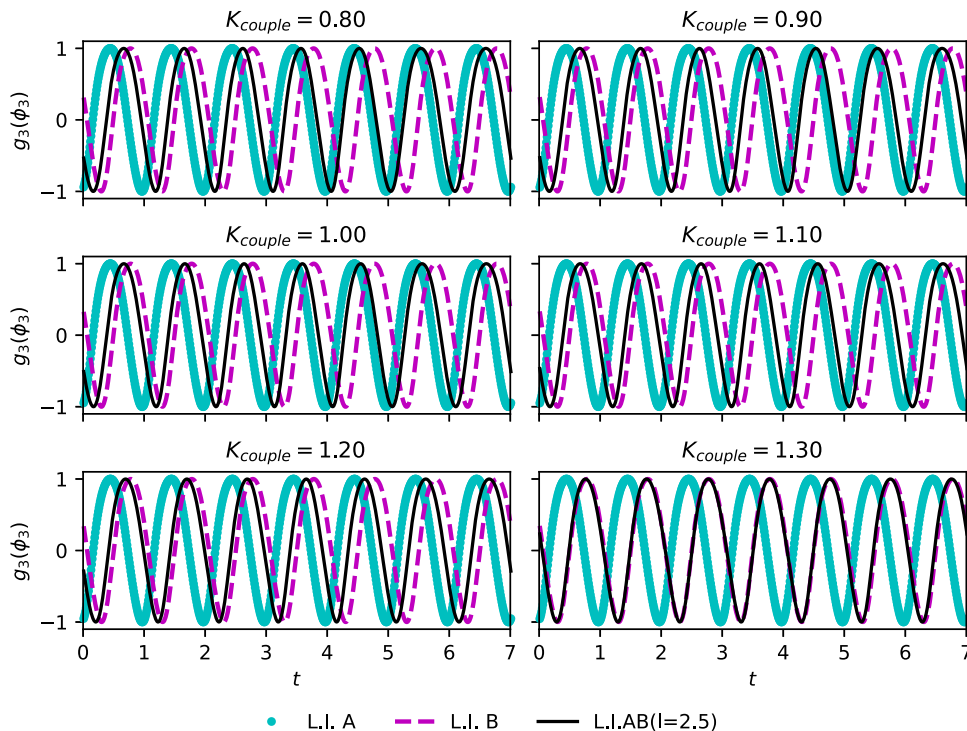
Fig. 2. The dotted cyan line corresponds to the output g3(ϕ_3) for the light input *A*, the dashed pink line for the light input *B* and the black continuous line for the light input *AB*(*l* = 2.5). In each panel the value of the coupling parameter K_{couple} is indicated.

space. In the next subsection we present the results for this question using a more general analysis.

4. Generalizing results

In this section, we present a more general analysis exploring the parameter space. We varied the parameter control K_{couple} responsible for the coupling between oscillators 1 and 2 and the parameter l that is the period of the week in which the light input $AB(l)$ coincides with light input B. We first analyze how the changes on K_{couple} and l affect the synchronization. We also estimate the period of the solutions, considering a Poincaré section on which we take one value per week. Finally, we make simulations following the attractors finding bistability for some parameters.

In order to have a more general view of the results, we calculate the modulus $R(\phi_{3AB(l)}, \phi_{3A})$, $R(\phi_{3AB(l)}, \phi_{3B})$ and the angles $\theta(\phi_{3AB(l)}, \phi_{3A})$, $\theta(\phi_{3AB(l)}, \phi_{3B})$ of the first moments from the distributions $z(\phi_{3AB(l)}, \phi_{3A})$ and $z(\phi_{3AB(l)}, \phi_{3B})$ for $l \in [0, 7]$ with a step of 0.0125 day and $K_{couple} \in [0.6, 1.3]$ with a step 0.00125. It is worth remembering here that the light input $AB(l)$ has $7 - l$ days in the light input A and l days in the light input B, and that there is a shift of 8 h between A and B. Therefore, we decide to vary l to verify if the behavior that we find for $l = 2.5$ and $K_{couple} = 1.3$ is usual or if it is an exception. We are also interested to observe if other phenomena could appear in these other sets of parameters. In Fig. 3 we present the results, in both cases in the axis x we have the coupling K_{couple} and in axis y l.

In Fig. 3 we basically see three types of behavior. The most common is the following: if the time for red light stimulus A is higher than B during the week, the output signal of the suprachiasmatic nucleus (SCN) ϕ_3 is better synchronized to the output correspondent to light input A than to the output correspondent to light input B and vice-versa. We can see this behavior comparing the parameters space on the Fig. 3 on the left (related to light input A) to the parameters spaces on the right (related to light input B). For $l < 3.5$, for the most values of K_{couple}, R is red larger on the left panel (related to light input A) than on the right panel (related to light input B), and θ is closer to 0 on the left panel than on the right panel, the regions where these properties do not occur will be explained later. Inversely, for $l > 3.5$, R is larger on the right panel (related to light input B) than on the left panel (related to light input A), and θ is closer to 0 on the right panel than on the left panel. It is important to notice that R could vary between 0 and 1. However, in our system even the cases that are less synchronized are far from being completely unsynchronized nsynchronized state with $R = 0$. We choose to limit the scale between 0.8 and 1 so the differences between the levels of synchronization can be visualized.

In a smaller area of the parameter space, the behavior is the opposite of the common. In this case we observe the same effect previously reported for the light input $AB(l = 2.5)$ with $K_{couple} = 1.3$. The regions where this behavior occurs are highlighted by continuous black borderlines.

There are also three areas where neither the common behavior nor its opposite clearly occur. These regions are highlighted in dashed white borderlines in Fig. 3, which we will call from now on regions Y. In these areas, the levels of synchronization are lower in general than in the rest of the parameter space and there is no much difference between the panels on the right and on the left. In each region Y the color patterns change abruptly in the colormaps of the lengths $R(\phi_{3AB(l)}, \phi_{3A})$ and $R(\phi_{3AB(l)}, \phi_{3B})$. In the colormaps of the angles $\theta(\phi_{3AB(l)}, \phi_{3A})$ and $\theta(\phi_{3AB(l)}, \phi_{3B})$ the variations are more subtle, even so it is possible to notice that in regions Y the color changes less regularly than in other regions.

Aiming to better identify what is happening in the regions Y, we simulate one of the regions Y with more details. In this sim-
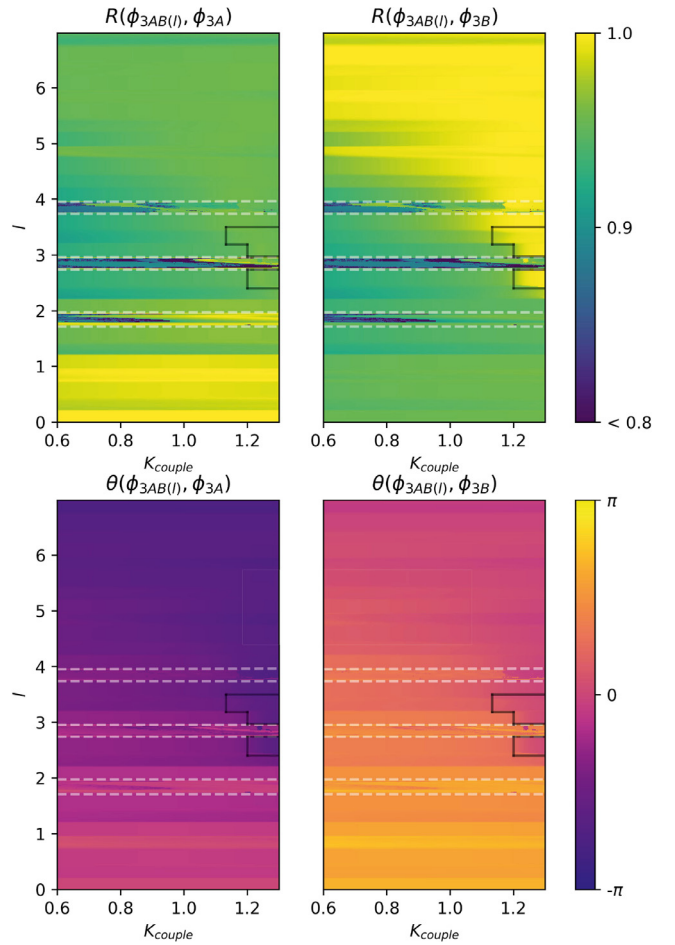
Fig. 3. Parameter spaces related to synchronization between $\phi_{3AB(l)}$ and ϕ_{3A} or ϕ_{3B}, which are, respectively, the phases of oscillator 3 when the light input is $AB(l)$, A, and B. $R(\phi_{3AB(l)}, \phi_{3A})[R(\phi_{3AB(l)}, \phi_{3B})]$ is a synchronization measurement between $\phi_{3AB(l)}$ and $\phi_{3A}[\phi_{3B}]$. $\theta(\phi_{3AB(l)}, \phi_{3A})$ $[\theta(\phi_{3AB(l)}, \phi_{3B})]$ is the mean angle between $\phi_{3AB(l)}$ and $\phi_{3A}[\phi_{3B}]$. K_{couple} is the control parameter, $l[7-l]$ is the number of days in the week that correspond to light input $B[A]$ in the light input $AB(l)$.

ulation K_{couple} changes in a step of 0.001 and l varies in a step of 0.005. We show the results in Fig. 4. We notice that region Y actually presents an intricate structure, that is similar (not identical) in both left and right panels for R. The same structure appears for θ, though the sign of the angles are opposite in the panels. While outside the regions Y the levels of coupling do not change much, or change smoothly with the changing of the K_{couple} or l, in the regions Y a slight change of parameter can change considerably the levels of synchronization. Also only in regions Y we find sets of the parameter space that assume the lowest values of synchronization in our scale.

The behavior in regions Y is more complicated, as a typical example we show the results for $l = 2.7750$ in Fig. 5. For questions of space in this figure we shortened $R(\phi_{3AB(l)}, \phi_{3A})$ as $R(ABA)$, $R(\phi_{3AB(l)}, \phi_{3B})$ as $R(ABB)$, $\theta_1(\phi_{3AB(l)}, \phi_{3A})$ as $\theta_1(ABA)$ and $\theta_1(\phi_{3AB(l)}, \phi_{3B})$ as $\theta_1(ABB)$. We also show the value that ϕ_3 assumes on the Poincaré section in which we save values at each 7 days $\phi_{3(7)}$. It is valid to remember here that the total period of the external forcing of this system is 7, since despite the changes during the week, at each 7 days the cycles re-initiates. Comparing $\phi_{3(7)}$ to $R(ABA)$, $R(ABB)$, $\theta_1(ABA)$ and $\theta_1(ABB)$ we notice that the abrupt changes of colors are related to bifurcations. Also, we can see regions with period 2, 4 and chaotic windows, the last ones being the regions with lowest values of $R(ABA)$ and $R(ABB)$.
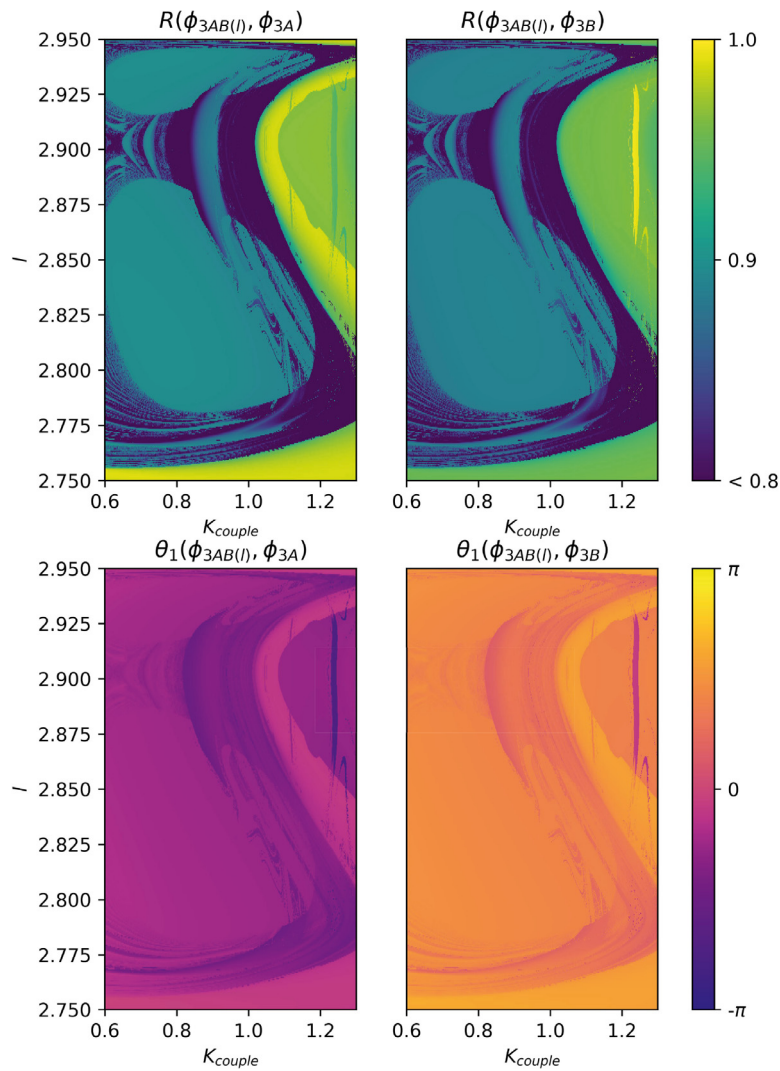
Fig. 4. Zoom of parameter spaces related to synchronization.
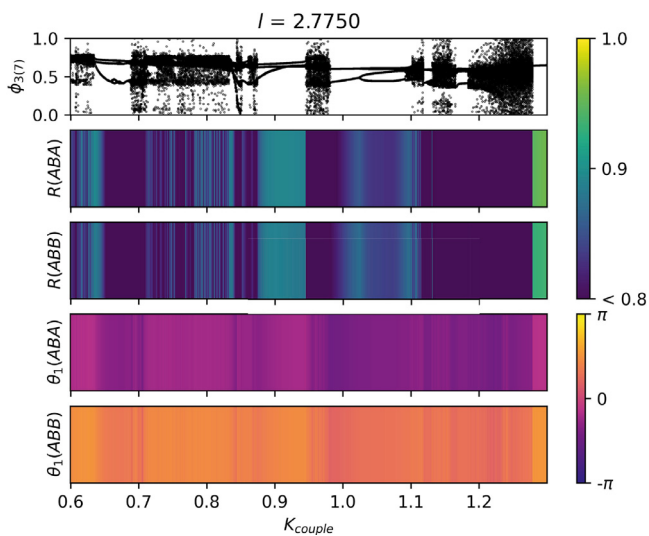
Fig. 5. $\phi_{3(7)}$ Value which ϕ_3 assumes on the Poincaré section in which we save values at each 7 days, abbreviation in figure $R(\phi_{3AB(l)}, \phi_{3A})$ as $R(ABA)$, $R(\phi_{3AB(l)}, \phi_{3B})$ as $R(ABB)$, $\theta_1(\phi_{3AB(l)}, \phi_{3A})$ as $\theta_1(ABA)$ and $\theta_1(\phi_{3AB(l)}, \phi_{3B})$ as $\theta_1(ABB)$.

Observing the value which ϕ_3 assumes on the Poincaré section (which we construct taking one value at each seven days) in Fig. 5 we already notice that in regions Y there are parameters which correspond to solutions with period 1, with period 2, while other parameters present much higher periods or even may be chaotic solutions. In order to analyze the periodicity of the solutions with more detail we present in Fig. 6 the period of the solutions firstly for the whole range on $l \in [0, 7]$ and $K_{couple} \in [0.6, 1.3]$, secondly for the same range of the Fig. 4 which we see that presents more intricate behavior. The color scale in the figure indicates the values of the periods, the white regions are the regions where algorithm is not able to find a period (either because the period is too high, or because the solution is chaotic). In the majority of the space we find period 1, but in the three regions that we find more complicated behavior other values of periods and white regions appear. In the second figure we also notice that the shape of the colorplot of the periods and of the quantities $R(\phi_{3AB(l)}, \phi_{3A})$, $R(\phi_{3AB(l)}, \phi_{3B})$ have similar shapes, which is reasonable, since when we look at one line in Fig. 5 the bifurcations and the abrupt changes of colors coincide. Another point to analyze is if there is bistability. To analyze that we simulate the system following the attractor, that is, using the final result of the simulation of one parameter as initial condition for the simulation for the next parameter. In these simulations the value of l is fixed
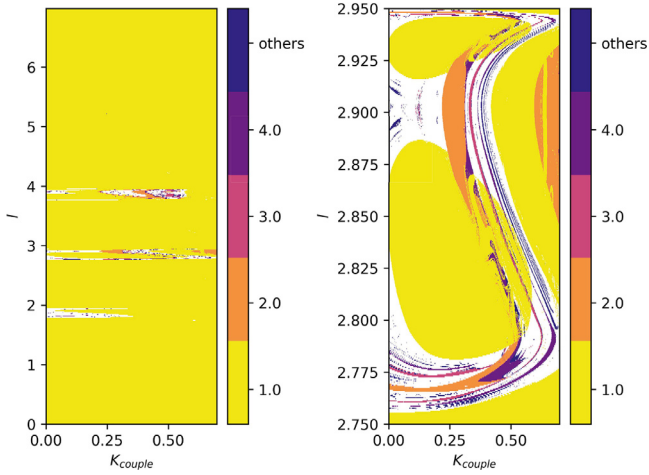
Fig. 6. Parameter space of the period. The white regions are the regions that the algorithm could not find a period, either because it is too high or because the solution is chaotic. The other periods are indicated in the legend next to the panels.
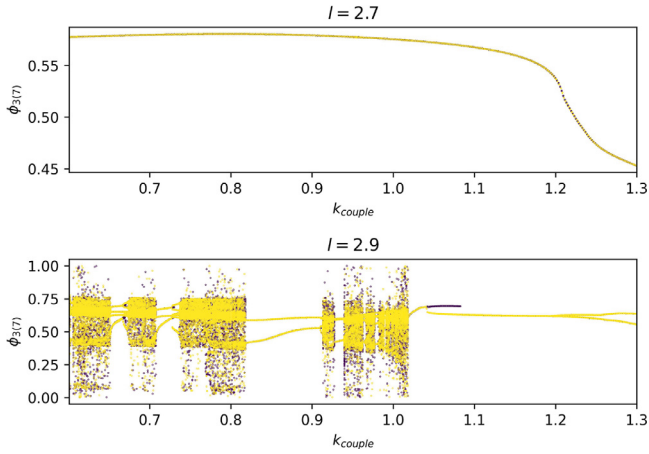
Fig. 7. Value that ϕ_3 assumes on the Poincaré section in which we take values at each seven days, for $l = 2.7$ and $l = 2.9$ following the attractor. In yellow (lighter gray on the impressed version) simulations with K_{couple} increasing and in purple (darker gray on the impressed version) decreasing.

and the value of K_{couple} is changed. We find out that for some values of l the attractor is the same when simulation is done with K_{couple}, increasing or decreasing. In Fig. 7 we show two examples: for $l = 2.7$ nothing changes, if the simulation is done with K_{couple} increasing or decreasing; for $l = 2.9$, though, there is a region in which we see bistability.

As a way to visualize this bistability better, we fixed the parameters $K_{couple} = 1.06$, $l = 2.9$ since from the Fig. 7 we know that these parameters belong to a region where bistability occurs.

In Fig. 8, we present a 2D slice of the basins of attraction. In principle, the complete basins of attractions would have dimension 4. However, in order to show the presence of bistability, a two dimensional slice of the region near to the fixed points in the basins of attractions is enough. Several criteria could have been used to select this slice, in the following we describe ours. First, we find the fixed points which are $s_0 = [8.66e - 02, 8.73e - 01, 6.79e - 01, 6.36e - 01]$ and $s_1 = [8.66e - 02, 2.34e - 01, 7.05e - 01, 6.96e - 01]$. The first direction of our slice is $m = [m_0, m_1, m_2, m_3] = s_1 - s_0$, the second direction is $n = [0, m_2, m_1, 0]$. The equation of the plan of this slice is $X = m*u + n*norm*v + s0$ with $norm = \frac{\sqrt{\sum_{i=0}^{4} m_i^2}}{\sqrt{\sum_{i=0}^{4} n_i^2}}$. Notice that when $(u, v) = (0, 0)$, $X = s_0$, and, when $(u, v) = (1, 0)$, $X = s_1$, so both fixed points belong to this slice.
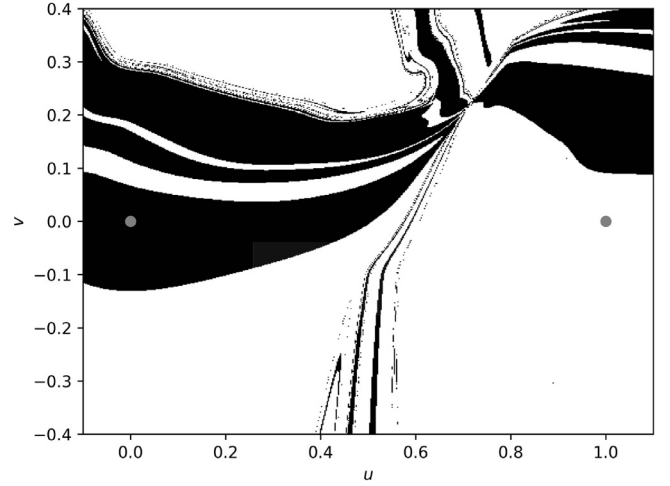
Fig. 8. 2D-slice of the basins of attraction for $K_{couple} = 1.06$ and $l = 2.9$ in the region near to the fixed points s_0 and s_1. The black dots are the fixed points. The initial conditions in the black(white) region converge for the fixed point in the black(white) region.

We also analyze the cases for different values of shifts between light inputs A and B. For lower values of shift we only find the common behavior, but as the shift increases we find the opposite behavior as well as areas with higher period and chaotic solutions. We present these results in the supplementary material. From those simulations, we conclude that different behaviors from the common one occur when the shift between the light inputs A and B is high enough.

We also simulate the system for $K_{couple} > 1.3$ even though these exceeds the limits used in [3]. More regions with solutions of higher period and chaos appear. Also we see an increase in the area of the region in which the opposite behavior of the common occurs, but the area in which this effect stands out more is visible in figures presented here. We add the figures for $K_{couple} > 1.3$ in the supplementary material.

5. Conclusions

We emulate the effect of social jetlag in the model introduced in [3], changing the light input by a light input sequence which represents a person's routine who suffers from social jetlag. The light input that we considered has a 7-days period and it is composed by a succession of two light inputs A and B. Both light inputs A and B are composed of 12 h of light and 12 h of dark, the only difference between them being a shift. The shift in the figures presented here is of 8 h, but we also analyzed other cases that we show in the supplementary material.

In reference [3], the authors found a simple relation, namely, the lower the coupling parameter the faster the recovery of the jetlag (shift in the light input). In our case, every week the system is subjected to a shift on the light input, so we made simulations to measure if the system is better synchronized to light input A (light input before the weekly shift) or to light input B (light input after the weekly shift). In order to improve our analyses we also determined the period of the solutions on a Poincaré section that we took one value per week. There was not a simple analogous of the result presented in [3]. However, we were able to find that there are regions in the parameter space where the output of the system is better synchronized in relation to light input A or B. We also highlighted the regions of the parameter spaces that differently from the rest have higher period and even chaotic solutions.

The most common behavior that we found was: if the individual spends more time under a light stimulus A(B) than B(A) during

the week, the output of the system is better synchronized to light input $A(B)$. However, in a small parameter space area, we also encountered the opposite behavior. It occurs due to the high non-linearity of the model. There is a minimal shift between the light inputs A and B which is needed for this behavior to appear.

We could not clearly identify either the common behavior or its opposite in some regions in the parameter space. In these areas small changes of parameters could lead to large variations on the levels of synchronizations. In these regions the lowest values of synchronization level of our simulation were reached. Almost the whole parameter space had solutions of period 1, the exceptions were exactly these regions where we saw solutions of higher periods or even chaotic solutions. Furthermore, for some parameters there is bistability. Again this type of behavior does not occur if the shift between the two light inputs is too short.

It would be very informative to find out if individuals under light inputs with systematic shifts, similar to those considered, present high period or chaotic output signals. Although it is possible to collect some data about people who suffer from social jetlag and analyze it, an experiment using mice would be very interesting, because then one could control the light input with precision as well as interfere in the coupling of the neurons. Also, it could be constructive to analyze how other models behave when subjected to the type of light input that we studied in this work.

Declaration of Competing Interest

The authors declare that they have no known competing financial interests or personal relationships that could have appeared to influence the work reported in this paper.

CRediT authorship contribution statement

Flávia M. Ruziska: Conceptualization, Formal analysis, Funding acquisition, Writing - original draft, Writing - review & editing, Methodology, Investigation. **Iberê L. Caldas:** Conceptualization, Formal analysis, Funding acquisition, Writing - original draft, Writing - review & editing, Supervision.

Acknowledgements

Supplementary material

References

[1] Reppert SM, Weaver DR. Coordination of circadian timing in mammals. Nature 2002;418(6901):935. doi:10.1038/nature00965.

[2] Xie Y, Tang Q, Chen G, Xie M, Yu S, Zhao J, et al. New insights into the circadian rhythm and its related diseases. Front Phys 2019;10:682. doi:10.3389/fphys.2019.00682.

[3] Yamaguchi Y, Suzuki T, Mizoro Y, Kori H, Okada K, Chen Y, et al. Mice genetically deficient in vasopressin V1a and V1b receptors are resistant to jet lag. Science 2013;342(6154):85. doi:10.1126/science.1238599. http://science.sciencemag.org/content/342/6154/85

[4] Lu Z, Klein-Cardeña K, Lee S, Antonsen TM, Girvan M, Ott E. Resynchronization of circadian oscillators and the east-west asymmetry of jet-lag. Chaos 2016;26(9):094811. doi:10.1063/1.4954275.

[5] Lee A, Galvez JC. Jet lag in athletes. Sports Health 2012;4(3):211.

[6] James SM, Honn KA, Gaddameedhi S, Van Dongen HP. Shift work: disrupted circadian rhythms and sleep—implications for health and well-being. Curr Sleep Med Rep 2017;3(2):104. doi:10.1007/s40675-017-0071-6.

[7] Knutsson A. Health disorders of shift workers. Occup. Med. 2003;53(2):103. doi:10.1093/occmed/kqg048.

[8] Oishi M, Suwazono Y, Sakata K, Okubo Y, Harada H, Kobayashi E, et al. A longitudinal study on the relationship between shift work and the progression of hypertension in male Japanese workers. J Hypertens 2005;23(12):2173.

[9] Torquati L, Mielke GI, Brown WJ, Kolbe-Alexander T. Shift work and the risk of cardiovascular disease. a systematic review and meta-analysis including dose–response relationship. Scand J Work EnvironHealth 2018;44 (3):229.

[10] Smarr BL, Schirmer AE. 3.4 million real-world learning management system logins reveal the majority of students experience social jet lag correlated with decreased performance. Sci Rep 2018;8(1):1. doi:10.1038/s41598-018-23044-8.

[11] Islam Z, Hu H, Akter S, Kuwahara K, Kochi T, Eguchi M, et al. Social jetlag is associated with an increased likelihood of having depressive symptoms among the Japanese working population: the Furukawa Nutrition and Health Study. Sleep 2019;43(1):zsz204. doi:10.1093/sleep/zsz204.

[12] Mota MC, Silva CM, Balieiro LCT, Gonçalves BF, Fahmy WM, Crispim CA. Association between social jetlag food consumption and meal times in patients with obesity-related chronic diseases. PLOS ONE 2019;14(2):1. doi:10.1371/journal.pone.0212126.

[13] Putilov AA, Verevkin EG. Simulation of the ontogeny of social jet lag: a shift in just one of the parameters of a model of sleep-wake regulating process accounts for the delay of sleep phase across adolescence. Front Physiol 2018;9:1529. doi:10.3389/fphys.2018.01529.

[14] Thomson F, Napier S. In: Stolerman IP, editor. Arginine-Vasopressin. Berlin, Heidelberg: Springer Berlin Heidelberg; 2010. p. 151. ISBN 978-3-540-68706-1

[15] Chang DC, Reppert SM. The circadian clocks of mice and men. Neuron 2001;29(3):555.